https://doi.org/10.1016/j.enggeo.2018.09.015

Spatial variability of saprolitic soil properties and relationship with joint set orientation of parent rock: insights from cases in Hong Kong

W.F. Liu, Y.F. Leung*

Department of Civil and Environmental Engineering, The Hong Kong Polytechnic University, Hung Hom, Hong Kong

Abstract

Geomaterials are known to be associated with significant heterogeneity, and the natural variations in properties can affect the occurrence of landslides and failure of engineering structures. While these variations are often observed to be spatially correlated, the correlation patterns and their relationships with the geological origins of the materials are not well understood. This study utilizes a three-dimensional spatial variability model to investigate the correlation features in mechanical properties of saprolitic soils, which are products of chemical weathering of granite. Rigorous geostatistical analyses are performed for soil test data at four locations in Hong Kong, each also consisting of extensive rock joint survey information. The analyses show that the principal directions of spatial variability in saprolitic soils correlate well with joint set orientations in the parent rock, providing quantitative evidence that soil heterogeneity partly arises from the different rates of weathering along various directions relative to the rock discontinuities.

Keywords: Spatial variability, Geostatistics, Saprolites, Weathering, In situ soil testing

*Corresponding author
Email address: andy.yf.leung@polyu.edu.hk (Y.F. Leung)

1. Introduction

Spatial variability in the properties of rocks and soils has been widely recognized (e.g., Jiang et al., 2014; Cho, 2007; Li et al., 2015a), and shown to be key factors for natural phenomena such as landslides (Griffiths et al., 2009; Fan et al., 2016; Huang et al., 2017b), or behavior of engineering structures including tunnels and building foundations (Cho, 2012; Al-Bittar and Soubra, 2014; Huang et al., 2017a; Lo and Leung, 2017). Currently, the patterns of soil spatial variability and their potential links with local geology are not well understood. This is partly attributed to the lack of soil and rock data required for rigorous spatial or geostatistical analyses. Meanwhile, there is limited discussion on methods to characterize the spatial correlations of soil data in the three-dimensional subsurface domain.

Various simplifying assumptions were made in previous studies of spatial variability. For example, the two-dimensional correlation model is often adopted in probabilistic analyses, considering horizontal and vertical correlations in soil properties (Li et al., 2015a, 2017; Bong and Stuedlein, 2018). Recently, three-dimensional spatial variability of soils has been taken into account in site characterization and geotechnical reliability assessments (Li et al., 2015b; Xiao et al., 2016; Leung and Lo, 2018; Xiao et al., 2018). It should be noted, however, that the variation patterns for soil properties may differ in three dimensions: soil layering usually refers to material properties being relatively uniform along the horizontal directions, while showing abrupt changes with depth. This may be the predominant feature for transported soils that had been deposited in horizontal

layers. On the contrary, saprolitic soils are products of chemical weathering of rock, so the mechanical properties and their spatial correlations may depend on geological features of the parent rock, including the presence and orientations of joints that influence the weathering process in various directions.

This study explores the relationship between spatial variability/correlations in mechanical properties of saprolitic soils and the joint set orientations of underlying parent rock, through three-dimensional geostatistical analyses at four separate locations in Hong Kong. The soil investigated is the completely decomposed granite (CDG) commonly encountered in the territory. At each study location, hundreds to thousands of borehole measurements are available regarding in situ soil properties and rock joint information. Using a numerical framework recently developed (Liu and Leung, 2018) for characterization of three-dimensional anisotropic spatial correlations, systematic analyses are performed on soil heterogeneity features to reveal the potential links with site geology.

2. Site locations and methodology

2.1. Local geology and data acquisition

Figure 1 shows the four study sites located in the Kowloon Peninsula in Hong Kong. The region is underlain by the Kowloon Granite and Mount Butler Granite, which are both Cretaceous intrusive rocks. During the late Cretaceous, the climate became progressively moister, and the rocks were subjected to deep weathering under hot and humid conditions (Shaw et al., 2010). The sea level fluctuated between glacial periods during the Quaternary, and began to rise rapidly following the end of the last glacial

period, reaching its present level in the region about 8,000 years ago (Sewell et al., 2009).

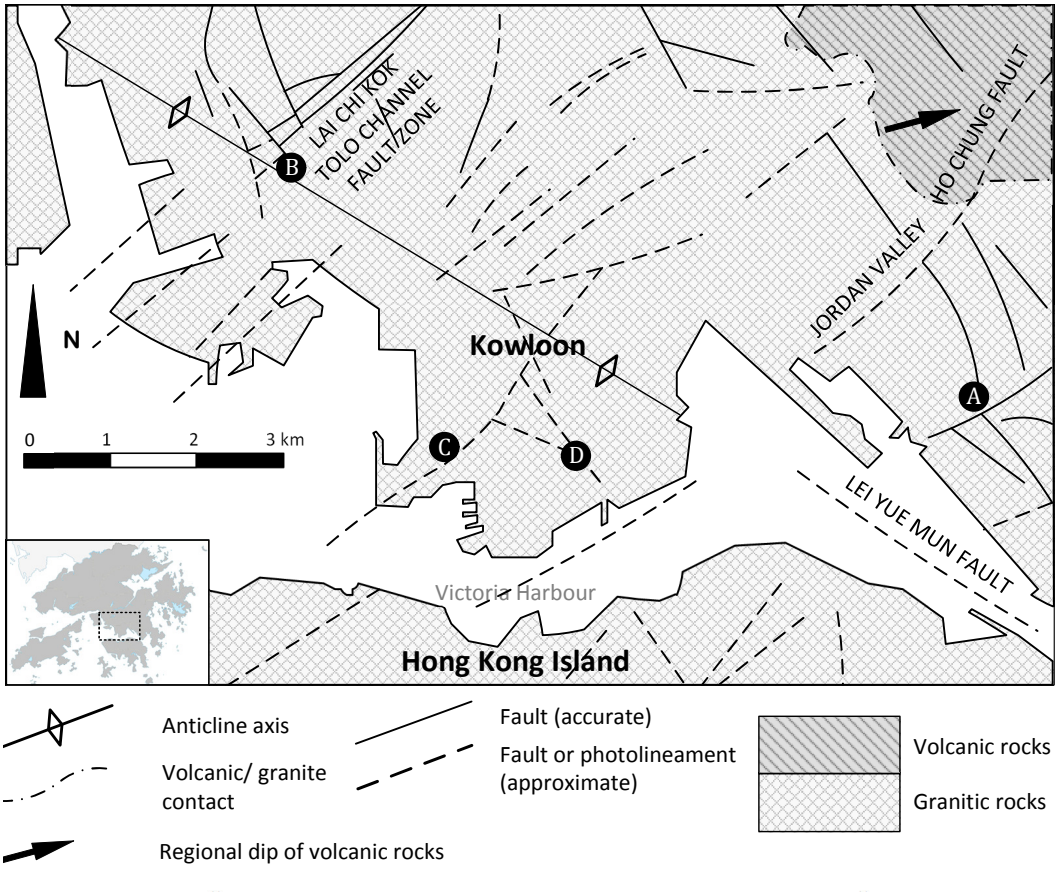

Figure 1: Local geology and locations of the four study sites.

The granite underlying the study area has undergone extensive decomposition by physical and chemical weathering, and is petrologically uniform both in texture and composition (Strange and Shaw, 1986). The parent rock is typically equigranular medium grained biotite monzogranite, and the dominant alkali feldspar is microcline with subordinate microperthite (Shaw, 1997). The fine-to-medium grained granite and associated fine-grained granite form small plutons, with the most prominent ones cropping out at Site A. At Site B, the coarse-grained granite is intruded by fine-grained granite. Sites

C and D are underlain by uniform medium-grained granite, and the main constituents are alkali feldspar, plagioclase and quartz. As shown in Figure 1, the local geology in the Peninsula involves a broad northwest-southeast (NW-SE) trending anticline plunging to the southeast, formed by volcanic rocks around the northeastern boundaries, with the core of such structure intruded by granites. The main trends in the faults are NW-SE and northeast-southwest (NE-SW) (Strange and Shaw, 1986). The major fault zone associated with the Lai Chi Kok-Tolo Channel Fault passes through the northwestern corner of the region (Burnett and Lai, 1985), with several parallel faults reported in different areas across the Peninsula. In addition, a southeast-dipping fault was exposed where Site B is located. The underlying granite appears closely jointed, and the NW-SE striking faults have produced some displacement of the NE-SW faults (Strange and Shaw, 1986). The southern parts of the Peninsula are dominated by NE trending fault which cuts through Site C, and a less significant NW trending fault may influence the nearby Site D. In the east, NW- and NE-striking faults cutting the granites near Site A are associated with zones of deep weathering, which produce distinctive linear topographic hollows.

The downward succession of typical strata at the sites consists of fill material overlying sandy marine and/or alluvial deposits, and saprolitic soil of various thickness underlain by the granitic bedrock. The saprolitic soil (CDG) can be briefly described as extremely weak to very weak greenish grey, completely decomposed, fine to coarse-grained granite, with some fine to medium gravel. Generally, this stratum is found at depths of about 10 to 14 m below existing ground level, with its thickness varying across each site, typically between 5 m to 25 m. In many parts of the Kowloon Peninsula, the groundwater level is

close to the ground surface. It was reported to be between 1 to 2 m below existing ground level in Site B, and around 5 m below ground surface at other sites.

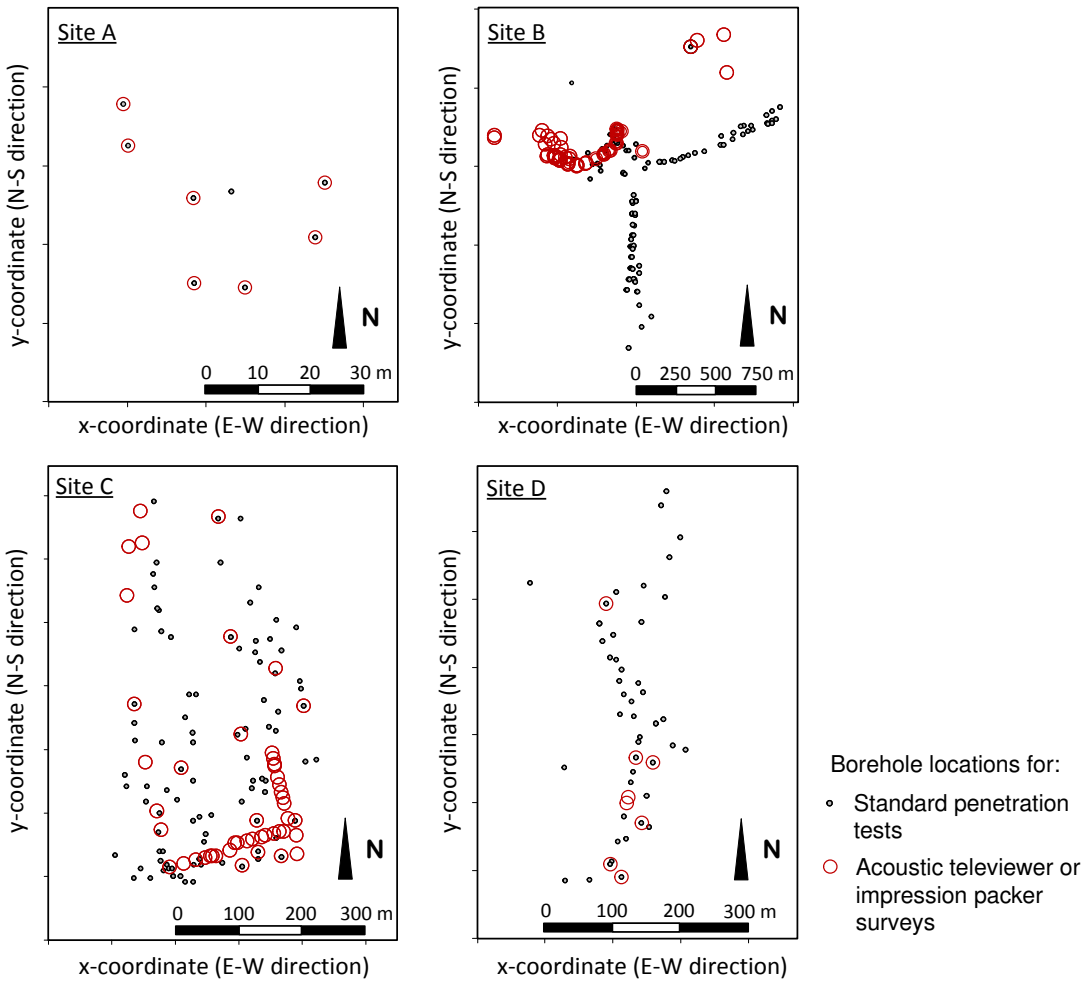

Figure 2: Distributions of boreholes at the four study sites.

Borehole records were obtained from geotechnical investigation reports of previous engineering projects in these areas, archived in the Civil Engineering Library of the Hong Kong Government. The boreholes are irregularly spaced across the study sites (Figure 2), with the closest spacing from less than 1 m to about 7 m at the four locations. Table 1

Figure 3: Photos of soil specimens and rock cores obtained at the four sites, with CDG marked by rectangles

presents the site information and number of in situ tests (size of dataset) performed to obtain the saprolitic soil properties and rock joint data, while Figure 3 shows photos

of the CDG and rock cores extracted from the sites. Standard penetration tests (SPT) were performed at various depths of each borehole, which involved a standard 140-pound hammer, falling from a drop height of 760 mm and hitting the drill rod connected to a sampler at depth. The SPT-N value represents the number of such hammer strikes required for the sampler to penetrate 300 mm into the soil at depth, and this value is found to be closely related to the mechanical properties of soils, including strength and stiffness (Kulhawy and Mayne, 1990; Clayton, 1995). Meanwhile, impression packer discontinuity surveys and acoustic televiewer surveys were performed within the rock mass in some of the boreholes, to identify the orientation and dip of existing joints in the granite. In this study, the spatial correlations of SPT-N values in three dimensions are analyzed for the CDG soil layer, and the results are interpreted in conjunction with the joint set orientations in the parent rock, to reveal potential connections between saprolitic soil properties, geological features and weathering patterns.

Table 1: Details of four study sites with soil and rock dataset.

Study site	Site area (m^2)	Number of boreholes	Size of dataset		Vertical interval of tests (m)
			SPT-N	Rock joint	
Site A	45 × 50	8	51	447	1.8 ∼ 2.0
Site B	2000 × 2500	165	534	2550	1.5 ∼ 2.0
Site C	350 × 750	141	495	1588	1.5 ∼ 3.5
Site D	300 × 1400	55	198	510	2.0 ∼ 3.0

2.2. Three-dimensional spatial variability model

As an indicator of geomechanical properties, SPT-N values in soil are usually observed to increase with depth from the ground surface, since soil strength and stiffness increase with geostatic stress levels. When modeled as spatial random variables, the N values are expressed as a combination of this trend and residuals (or deviations from the trend), with the latter being spatially correlated: the N values at two locations i and j are similar to each other when the separation distance is small between the points, even without considering the trend effects. With the vector $\boldsymbol{x}$ representing spatial coordinates of the sampled points, and vector $\boldsymbol{z}$ denoting the spatially-variable N values at those locations, a general linear mixed regression model for the spatial data, $\boldsymbol{z}$, can be formulated by:

$$\boldsymbol{z}(\boldsymbol{x}) = \mathbf{X}\boldsymbol{\beta} + \boldsymbol{\varepsilon} \tag{1}$$

where $\mathbf{X}\boldsymbol{\beta}$ represents the large-scale trend: $\mathbf{X}$ is the deterministic component matrix formed by the spatial coordinates, and $\boldsymbol{\beta}$ is the vector of regression coefficients according to the trend structure (e.g., linear, quadratic or cubic polynomial). The order of trend structure should be carefully determined to achieve good predictive capability and avoid overfitting the data at the same time. To obtain the optimal trend order, this study adopts the integrated approach discussed in detail by Liu et al. (2017), and the procedures are also described briefly in the appendix. Apart from Site B, where cubic trend order is adopted, the remaining 3 cases involve quadratic trends for SPT-N values.

The residuals, $\boldsymbol{\varepsilon}$, include components of smooth scale variation (with variance σ_e) that changes with distance, and also random white noise (with variance σ_n). The white noise

effects may arise from measurement errors associated with the in situ tests, which are assumed not to correlate with distance. The covariance matrix of $\boldsymbol{\varepsilon}$ is denoted as $\mathbf{V}$, and is given by (Liu and Leung, 2018):

$$\mathbf{V} = \mathbf{Var}(\boldsymbol{\varepsilon}) = \sigma_e^2\mathbf{R} + \sigma_n^2\mathbf{I} = (\sigma_e^2 + \sigma_n^2)\,[s\mathbf{R} + (1-s)\mathbf{I}]$$

$$\text{where } \; 0 \leq s = \frac{\sigma_e^2}{\sigma_e^2 + \sigma_n^2} \leq 1 \tag{2}$$

In equation (2), $\mathbf{I}$ is the identity matrix, and s is the spatial dependence parameter which incorporates the white noise effects into the covariance model; the $\mathbf{R}$ matrix represents the autocorrelation structure, which models the variation of $\boldsymbol{\varepsilon}$ in the spatial domain. In this study, the three-dimensional variations of N values are investigated, and the components of $\mathbf{R}$ are modeled by the squared exponential function, the basic form of which is as follows:

$$R_{ij} = \exp\left(-\frac{h_x^2}{\theta_x^2} - \frac{h_y^2}{\theta_y^2} - \frac{h_z^2}{\theta_z^2}\right) \tag{3}$$

where h_x, h_y and h_z are the separation distances between locations i and j, along the x, y and z directions, respectively; θ_x, θ_y and θ_z are the autocovariance distances in the three directions, beyond which the correlations between two points become insignificant. They may be interpreted as 'influence ranges' of the spatial correlations. Through equation (3), correlations of soil properties are defined along the x, y and z directions, and Liu and Leung (2018) further showed that with this form of separable correlation function, the autocovariance distances (θ) for other orientations can be represented by an ellipsoid (Figure 4a).

In this study, the principal directions of spatial correlation represent three orthogonal

directions, with the major direction (largest θ value) associated with the smoothest variation in soil properties. Along the minor principal direction, the properties vary most rapidly. This definition was also adopted by Zhu and Zhang (2013), and later by Liu and Leung (2018), and the model allows anisotropy in the spatial variations to be considered, meaning that the variability features can differ along various directions. In general, the horizontal and vertical axes may not represent the principal directions of spatial correlations (Figure 4b), which should depend on the depositional history of the geomaterial and/or geological history of the region. In fact, the main focus of this study is to investigate the principal directions of spatial correlations in saprolitic soils, and to compare them with joint data of the underlying parent rock. For this purpose, the framework adopted here (Liu and Leung, 2018) considers the rotations of principal axes, whereby the components of $\mathbf{R}$ matrix become:

$$R_{ij}^{*} = \exp\left(-\frac{h_1^2}{\theta_1^2} - \frac{h_2^2}{\theta_2^2} - \frac{h_3^2}{\theta_3^2}\right)$$

$$\text{where } \begin{Bmatrix} h_1 \\ h_2 \\ h_3 \end{Bmatrix} = \mathbf{\Omega}_3\mathbf{\Omega}_2\mathbf{\Omega}_1 \begin{Bmatrix} h_x \\ h_y \\ h_z \end{Bmatrix}$$

$$\mathbf{\Omega}_1 = \begin{bmatrix} \cos\alpha_1 & \sin\alpha_1 & 0 \\ -\sin\alpha_1 & \cos\alpha_1 & 0 \\ 0 & 0 & 1 \end{bmatrix}; \quad \mathbf{\Omega}_2 = \begin{bmatrix} \cos\alpha_2 & 0 & -\sin\alpha_2 \\ 0 & 1 & 0 \\ \sin\alpha_2 & 0 & \cos\alpha_2 \end{bmatrix};$$

$$\mathbf{\Omega}_3 = \begin{bmatrix} 1 & 0 & 0 \\ 0 & \cos\alpha_3 & \sin\alpha_3 \\ 0 & -\sin\alpha_3 & \cos\alpha_3 \end{bmatrix} \tag{4}$$

and α_3, α_2 and α_1 represent the rotation angles about x, y and z-axes, respectively; θ_1,

153 θ_2 and θ_3 are autocovariance distances along the principal axes after rotation, and h_1, h_2
154 and h_3 are the separation distances in the corresponding directions.

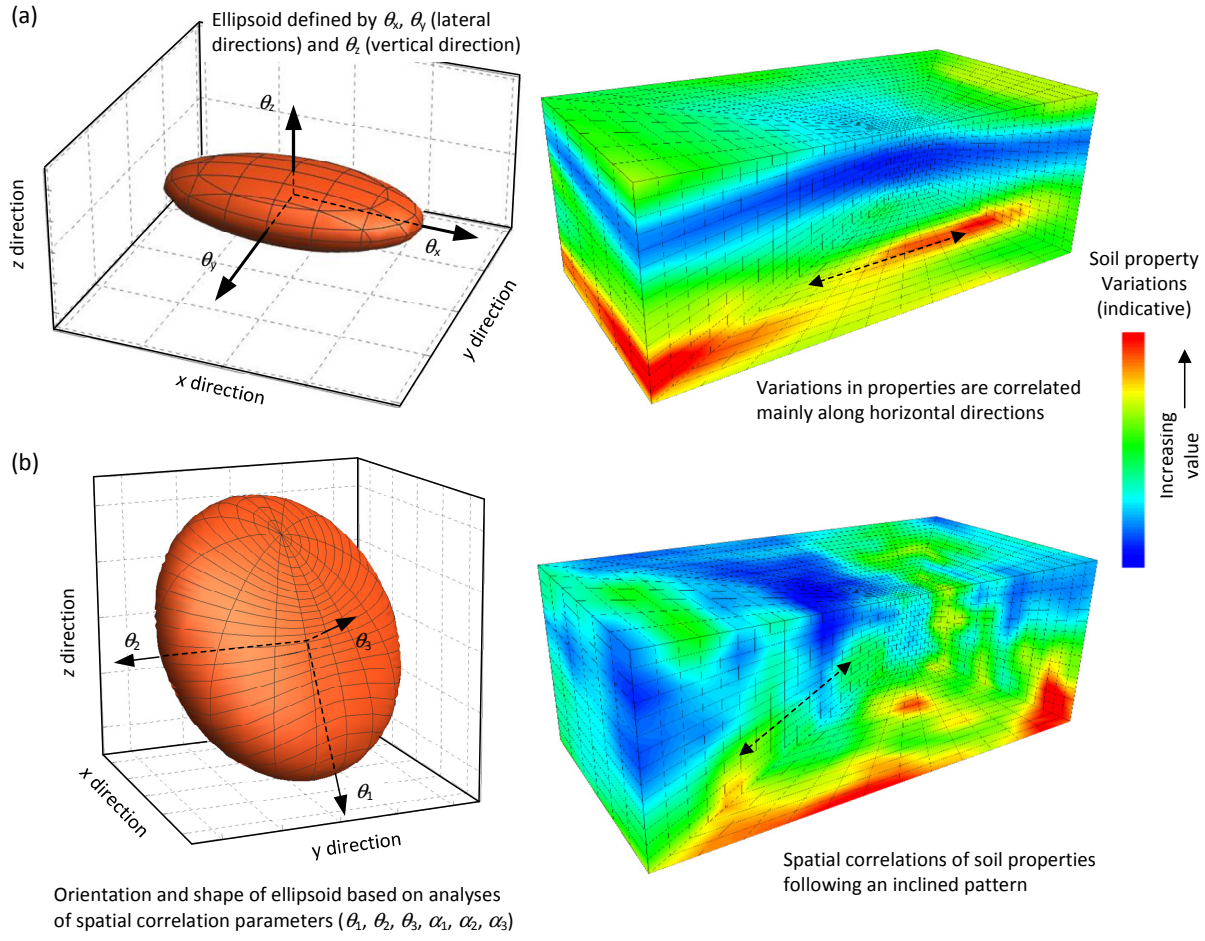

Figure 4: Illustration of ellipsoids of θ parameters (left) and the corresponding variability features in soil properties (right). Besides the general trend showing an increase with depth, local variations may follow different correlation patterns: (a) layered soils with horizontal and vertical axes being principal directions; (b) rotated principal directions of correlation.

155 To investigate the site-specific features of spatial variability in saprolitic/residual
156 soils, it is necessary to estimate the associated parameters at the four study sites, using
157 sampled SPT-N values in the CDG soil layer. In other words, the trend coefficients, $\boldsymbol{\beta}$

(equation (1)), and spatial correlation parameters s (equation (2)), α_1, α_2, α_3, θ_1, θ_2 and θ_3 (equation (4)) need to be determined based on observed values of $\boldsymbol{z}$ at the sites. This study employs the restricted maximum likelihood method, which searches for the set of parameters leading to the largest probability of matching the observed SPT-N data. The approach is briefly described in the appendix, with the mathematical details described in Cressie and Lahiri (1996) and Liu et al. (2017).

In cases where θ along the minor principal direction is significantly shorter than those in other directions, the resulting ellipsoid will resemble a planar surface, with a prevailing 'strike' (or dip direction, γ, which is orthogonal to strike line) and 'dip' angle (ϕ) in the three-dimensional space. This allows the orientations to be represented by stereographic projection, and to be compared directly with the stereoplot of joint set orientations of the parent rock underneath. This process is shown in Figure 5, where the direction normal to the planar ellipse is represented by the pole point on the horizontal projection plane. The theoretical details of stereographic projections can be found in Priest (1985) and Lisle and Leyshon (2004), etc., while the implications of this representation of soil spatial variability will be discussed further in the next section.

3. Results and Discussions

Table 2 summarizes the estimated parameters from spatial variability analyses of saprolitic soils at the four study sites. Orientations and shapes of the corresponding ellipsoids are also shown graphically in Figure 6. In all four cases, θ in the minor principal direction is significantly shorter than the other directions. The resulting ellipsoids resem-

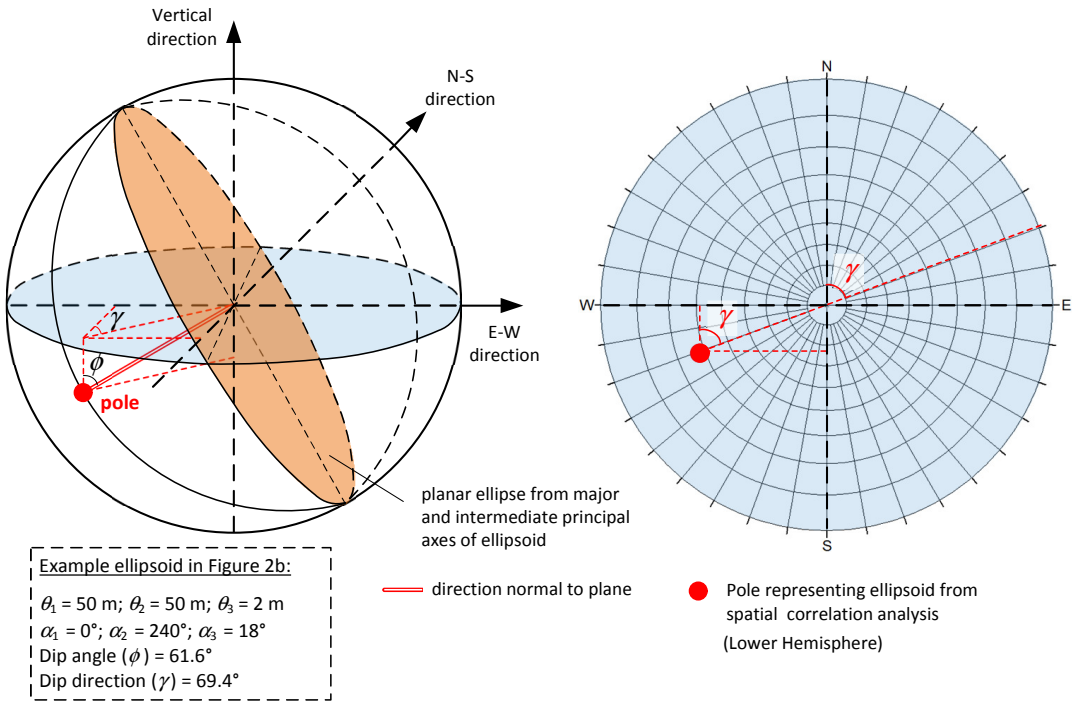

Figure 5: Representation of ellipsoid from spatial correlation analyses by the stereographic projection, using the example from Figure 4b.

ble planar surfaces, with the lower-hemisphere stereographic projections also plotted and compared with joint set surveys of the underlying granitic rock. It should be noted that the poles representing individual rock joint planes are plotted with the same technique as the ellipsoid of spatial variability (Figure 5), so that the contours shown in Figure 6 illustrate the predominant dip directions and angles of major joint sets in the granite.

Through Figure 6, the spatial correlation features in the CDG soil can be interpreted together with the geological settings of the study sites. For Sites A and B, the NW- and NE-striking faults cutting the granites lead to the similar trending joint sets. The ellipsoids from the corresponding spatial correlation analyses (Figure 6a and b) are also

Table 2: Spatial variability parameters for SPT-N values in CDG at four study sites.

Study site	Spatial	Autocorrelation distance (m)			Rotation of axes (deg)		
	dependence, s	θ_1	θ_2	θ_3	α_1	α_2	α_3
Site A	0.99	1.3	51.3	32.7	354	49	331
Site B	0.77	4.1	20.0	35.4	59	251	357
Site C	0.62	11.5	3.8	140.3	21	261	173
Site D	0.75	4.2	200.0	24.5	37	219	178

associated with dip directions and angles which correlate well with the major joint sets of granitic rock underneath. The connections between spatial variability observed in weathered materials and joint set orientations of the parent rock may be attributed to the mechanism of chemical weathering. The weathering process is promoted by groundwater flow along pre-existing discontinuities within the rock mass, and is influenced by changes in groundwater table over geological time and also during the seasonal wetting and drying cycles (GEO, 2007). The degree of decomposition varies in three dimensions, with the weathering process concentrating along the joints but showing more variations as it progresses into the rock mass through microfractures. Consequently, larger variations can be expected for the decomposed geomaterials in the direction normal to the joint plane, and hence a shorter spatial correlation range (θ) along that direction for saprolitic or residual soil properties. This relationship between saprolitic soil properties and rock joint orientations is conspicuous for Sites A and B considering the similar dip directions

and angles associated with the ellipsoid and the major joint set.

At Site C, the SPT-N values in CDG reveal significantly longer correlation range along the vertical direction, and the ellipsoid appears as a vertical planar surface. The rock joint survey also shows similar NE-SW trending sub-vertical joint set, although the dipping angle is slightly different. In fact, the pole representing the ellipsoid is close to the cluster of NE-SW trending, sub-vertical rock joint poles, marked by the red boundary in Figure 6c. On the other hand, the comparisons appear less promising for Site D, as shown in Figure 6d. In this case, although the dip angles of ellipsoid (from spatial variability analyses) and major rock joint systems do not match with each other, the strike of the two compare quite well, as shown by the Rosette diagrams in Figure 7. This angle also matches with the NW-SE trending fault system in the regions surrounding Site D, as illustrated in Figure 1. In fact, for all the four study sites, Figure 7 shows that the orientations for major axes of CDG variations generally follow the strikes of the joint geometric pattern.

Although the directions of saprolitic soil variability generally match with the rock joint orientations, there are several factors that can cause discrepancies to various extents. Firstly, statistical uncertainty is a common issue in many endeavours of geotechnical data analyses. This refers to the difficulties of obtaining the 'actual' statistical properties due to the limited amount of data, i.e., the small number of samples compared with the vast unsampled regions of the site. For example, Site A contains a relatively small number of SPT-N values for spatial analyses. This study adopts the restricted maximum likelihood method, which had been shown to be more robust than other geostatistical techniques

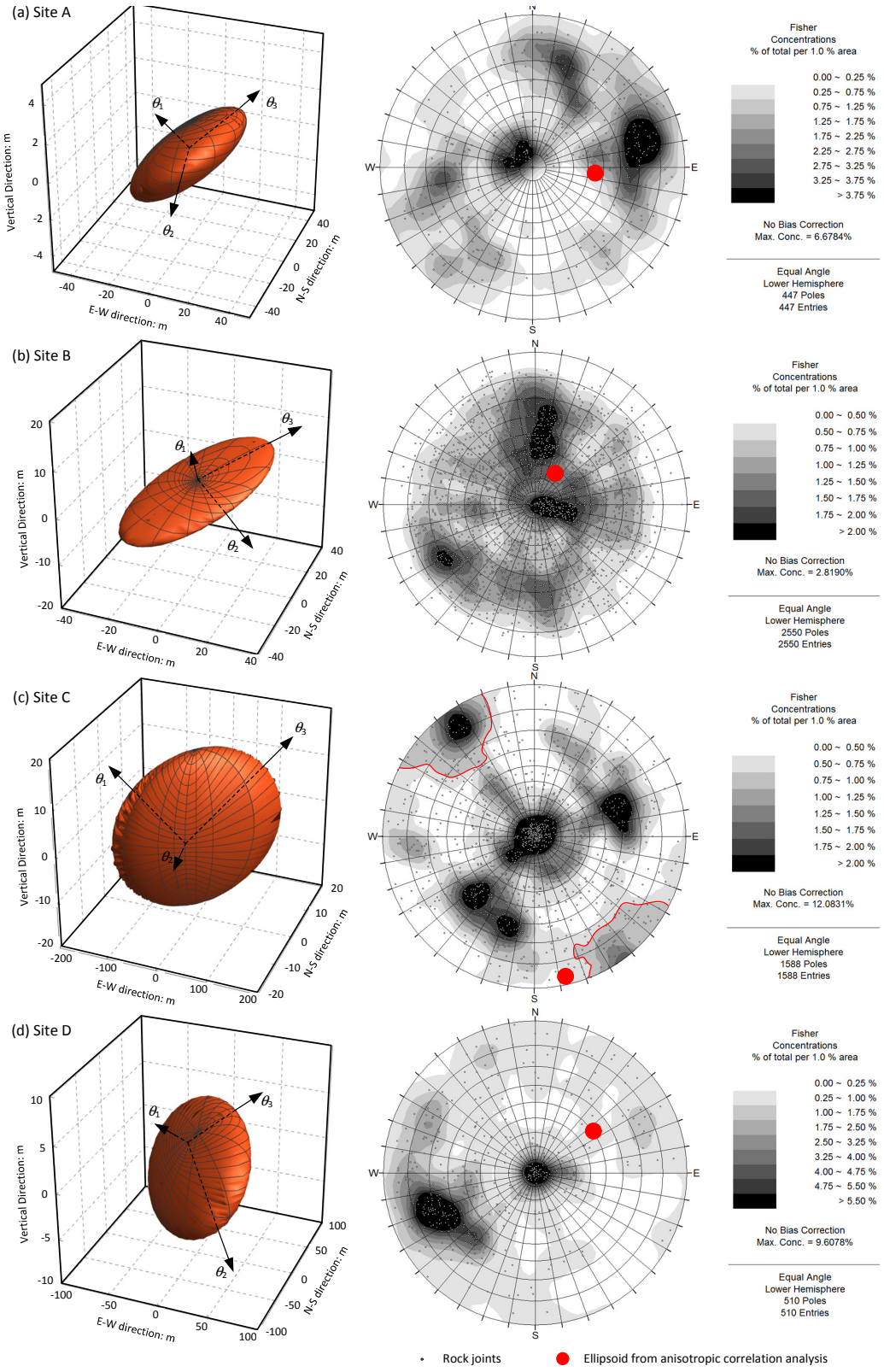

Figure 6: Ellipsoids of θ parameters from spatial variability analyses (left), and comparisons of their poles with rock joint data on stereographic projections (right).

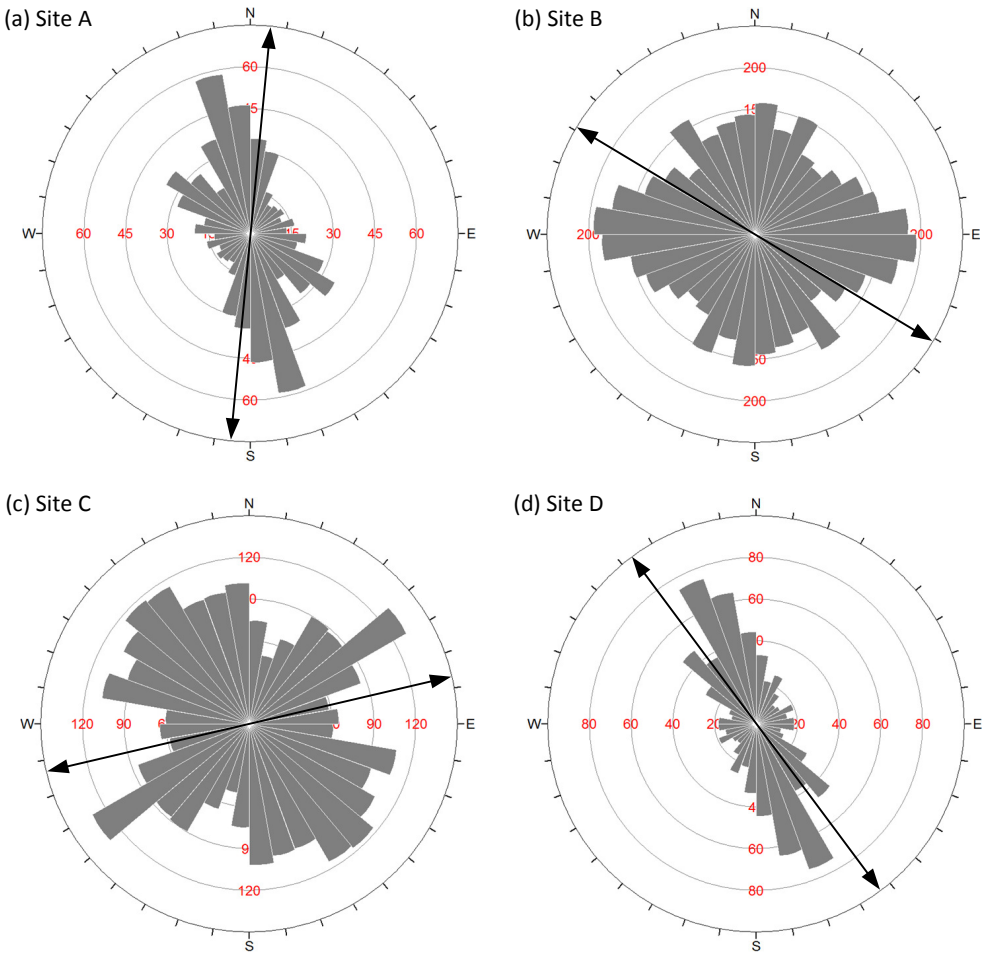

Figure 7: Rosette diagrams of strike from joint sets records (gray bars) and orientations of ellipsoids (arrows) from spatial correlation analyses of SPT-N values at the four sites.

(Cressie, 1993; Liu et al., 2017). However, when the samples are very limited, Bayesian methods may produce more consistent results for site characterizations, as discussed by Ching et al. (2016). Nonetheless, statistical uncertainty exists regardless of the analysis approach, and may contribute to the fact that the spatial correlation directions do not perfectly match the rock joint data.

The potential limitations of soil and rock testing methods associated with this study should also be noted. Parts of the rock joint data at the four sites were obtained through acoustic televiewer surveys, which involve acoustic signals being emitted from within the borehole, and the features of returning signals were measured and used to provide an unwrapped 360-degree digital image around the borehole wall. The discontinuities can then be identified around the borehole wall. While this is particularly useful in identifying interpanel or intercolumn joints, the method can be less effective in capturing steeply dipping, vertical or sub-vertical joints around a vertical borehole (Park and West, 2002; Bruce, 2012). It is therefore possible that sampling bias is present in the rock joint data regarding the steeply dipping discontinuities. In addition, while the SPT is very commonly performed in engineering projects in Hong Kong, giving rise to the large volumes of in situ soil testing data, their results may be affected by inconsistencies arising from different operators of the equipment and different site conditions. Therefore, the four study sites in this paper are carefully selected from relatively recent projects, where the tests were performed using mechanized hammer systems associated with improved consistency.

In addition, there can be physical reasons behind the observed discrepancies. Apart from orientations of rock discontinuities, the mineral compositions of the parent rock also affects the rate of weathering. Local variations in mineralogical content within the rock mass may therefore lead to preferential weathering, along directions other than the joint set orientations. Although this is a possible factor influencing the principal directions of soil spatial variability, this is admittedly very difficult to verify from data of saprolitic soils, since the rock fabric has already been broken down.

4. Conclusions

The presented three-dimensional spatial variability model allows rigorous geostatistical analyses to be performed with subsurface exploration data, in order to reveal the correlation features of geomaterials. Through the analyses on thousands of soil and rock testing data, this study shows that spatial correlation patterns in saprolitic soils are related to the joint set orientations of the parent rock, which controls the weathering process in various directions. This is manifested in the principal directions of soil spatial variability that coincide with the strike and/or dip angles of rock joints observed at the four study sites in Hong Kong. While this study focuses on saprolitic soils and the underlying granitic rock, it is quite possible that the spatial variations displayed in sedimentary soils may be related to the directions of discontinuities in sedimentary rocks, although further investigations will be necessary for this type of geomaterials.

The findings in this study enhance our understanding of the processes that lead to the natural variability of soil properties, which is an important factor in the occurrence of natural phenomena such as landslides and various applications of engineering geology. For example, Zhu et al. (2018) showed that directions of spatial correlations can have significant impacts on the safety factors of slopes, while Leung and Lo (2018) also demonstrated the importance of three-dimensional spatial variability in evaluations of foundation settlements and potentials of tilting. This study elucidated the geological origins of spatial patterns observed in soils, which should be crucial considerations when analyzing geotechnical data and understanding its implications for engineering projects.

Acknowledgments

The authors would like to thank C.H. Chong for his assistance in compiling and analyzing the data from Site A. The work presented in this paper is financially supported by the Research Grants Council of the Hong Kong Special Administrative Region (HKSAR) (Project No. 25201214). Also, the authors would like to acknowledge the permission of the Civil Engineering and Development Department, the Government of HKSAR, to present information and analyses of data obtained from government projects, archived in the Civil Engineering Library. Ownership of the data belongs to the HKSAR government, and readers may contact the authors for details of the four cases.

Appendix A.

The three-dimensional spatial correlation features of SPT-N values are characterized by the trend coefficients $\boldsymbol{\beta}$, and parameters s, θ_1, θ_2, θ_3 and α_1, α_2, α_3. These unknown parameters can be grouped into a vector $\boldsymbol{\Theta}$, and determined by the restricted maximum likelihood method, which involves maximization of the following log-likelihood function with respect to $\boldsymbol{\Theta}$:

$$L(\boldsymbol{\Theta}|\boldsymbol{y}) = -\frac{n-p}{2}\log(2\pi) - \frac{1}{2}\log|\mathbf{V}| - \frac{1}{2}\log|\mathbf{W}| - \frac{1}{2}\boldsymbol{y}^T\mathbf{V}^{-1}\mathbf{Q}\boldsymbol{y}$$

where $\mathbf{W} = \mathbf{X}^T\mathbf{V}^{-1}\mathbf{X}$

$$\mathbf{Q} = \mathbf{I} - \mathbf{X}\mathbf{W}^{-1}\mathbf{X}^T\mathbf{V}^{-1} \tag{A.1}$$

In equation (A.1), n is the number of sampled data points, and p is the number of coefficients in the trend structure; while $\boldsymbol{z}$ contains the sample values, $\mathbf{X}$ is composed of

the spatial coordinates, and the size of this matrix depends on the order of trend function. For example, if a three-dimensional linear trend (i.e., 4 regression coefficients) is to be determined for 50 data points, $\mathbf{X}$ will become a 50×4 matrix; $\boldsymbol{y} = (\mathbf{I}\text{-}\mathbf{X}(\mathbf{X}^T\mathbf{X})^{-1}\mathbf{X}^T)\boldsymbol{z}$ is the vector of filtered dataset (observations) with the trend components filtered out. The $\mathbf{V}$ matrix depends on the autocorrelation matrix $\mathbf{R}$, which is in turn dependent on the $\boldsymbol{\Theta}$ parameters through equations (2) to (4).

Determination of the correlation parameters consists of two interrelated steps: (i) maximization of $L(\boldsymbol{\Theta}|\boldsymbol{y})$ and (ii) selection of the trend order, which in turn affects $\boldsymbol{y}$. In this study, these are performed in a sequential manner. The linear trend is first assumed in $\mathbf{X}$ and $\boldsymbol{y}$, after which the corresponding log-likelihood function is maximized:

$$\boldsymbol{\Theta}^* = \arg\max_{\boldsymbol{\Theta}} L(\boldsymbol{\Theta}|\boldsymbol{y}) \tag{A.2}$$

where $\boldsymbol{\Theta}^*$ represents the vector of spatial correlation parameters that best represent the observed data. The maximization process can be treated as an optimization problem, which is solved in this study using an evolutionary algorithm known as differential evolution (Storn and Price, 1997). After obtaining $\boldsymbol{\Theta}^*$ for the linear trend ($\boldsymbol{\Theta}_1^*$), the process described by equations (A.1) and (A.2) is repeated with the quadratic trend to obtain $\boldsymbol{\Theta}_2^*$. The predictive capabilities of the two sets of correlation parameters ($\boldsymbol{\Theta}_1^*$ versus $\boldsymbol{\Theta}_2^*$) are then compared by the "leave-one-out cross-validation" method, which involves removing one observation at a time from the dataset, and then predicting its value using the remaining data and quantifying the associated error. In general, these steps are repeated until a higher order trend no longer leads to better predictive capability in the

model. Details of this procedure have been presented by Liu et al. (2017), and this avoids incorporation of an unnecessarily high trend order that may lead to overfitting of data.

Upon determination of the optimal trend order and the corresponding $\boldsymbol{\Theta}^*$ vector, the autocovariance distances along principal directions (θ_1,θ_2,θ_3) and their orientations in the three-dimensional domain can be established (α_1,α_2,α_3), through which the ellipsoids can be plotted.

References

Al-Bittar, T., Soubra, A.H., 2014. Probabilistic analysis of strip footings resting on spatially varying soils and subjected to vertical or inclined loads. J. Geotech. Geoenviron. 140, 04013043.

Bong, T., Stuedlein, A.W., 2018. Efficient methodology for probabilistic analysis of consolidation considering spatial variability. Eng. Geol. 237, 53–63.

Bruce, D.A., 2012. Specialty construction techniques for dam and levee remediation. CRC Press.

Burnett, A.D., Lai, K.W., 1985. A review of photogeological lineaments in Hong Kong. Geological Aspects of Site Investigations 2, 113 – 131.

Ching, J., Wu, S.S., Phoon, K.K., 2016. Statistical characterization of random field parameters using frequentist and Bayesian approaches. Can. Geotech. J. 53, 285–298.

Cho, S.E., 2007. Effects of spatial variability of soil properties on slope stability. Eng. Geol. 92, 97–109.

Cho, S.E., 2012. Probabilistic analysis of seepage that considers the spatial variability of permeability for an embankment on soil foundation. Eng. Geol. 133, 30–39.

Clayton, C.R.I., 1995. The standard penetration test (SPT): methods and use. CIRIA report 143, Construction Industry Research and Information Association, United Kingdom.

Cressie, N., Lahiri, S.N., 1996. Asymptotics for REML estimation of spatial covariance parameters. J. Statist. Plann. Inference 50, 327–341.

Cressie, N.A.C., 1993. Statistics for Spatial Data (Revised Edition). John Wiley & Sons.

Fan, L., Lehmann, P., Or, D., 2016. Effects of soil spatial variability at the hillslope and catchment scales on characteristics of rainfall-induced landslides. Water Resour. Res. 52, 1781–1799.

GEO, 2007. Engineering geological practice in Hong Kong. Geotechnical Engineering Office, Civil Engineering and Development Department, The Government of Hong Kong Special Administrative Region.

Griffiths, D.V., Huang, J., Fenton, G.A., 2009. On the reliability of earth slopes in three dimensions. Proc. R. Soc. A-Math. Phys. Eng. Sci. 465, 3145–3164.

Huang, H.W., Xiao, L., Zhang, D.M., Zhang, J., 2017a. Influence of spatial variability of soil Young's modulus on tunnel convergence in soft soils. Eng. Geol. 228, 357 – 370.

Huang, J., Fenton, G., Griffiths, D., Li, D., Zhou, C., 2017b. On the efficient estimation of small failure probability in slopes. Landslides 14, 491–498.

Jiang, S.H., Li, D.Q., Zhang, L.M., Zhou, C.B., 2014. Slope reliability analysis considering spatially variable shear strength parameters using a non-intrusive stochastic finite element method. Eng. Geol. 168, 120–128.

Kulhawy, F.H., Mayne, P.W., 1990. Manual on estimating soil properties for foundation design. Electric Power Research Institute, California.

Leung, Y.F., Lo, M.K., 2018. Probabilistic assessment of pile group response considering superstructure stiffness and three-dimensional soil spatial variability. Comput. Geotech. 103, 193 – 200.

Li, D.Q., Jiang, S.H., Cao, Z.J., Zhou, W., Zhou, C.B., Zhang, L.M., 2015a. A multiple response-surface method for slope reliability analysis considering spatial variability of soil properties. Eng. Geol. 187, 60–72.

Li, X.Y., Zhang, L.M., Gao, L., Zhu, H., 2017. Simplified slope reliability analysis considering spatial soil variability. Eng. Geol. 216, 90–97.

Li, Y.J., Hicks, M.A., Nuttall., J.D., 2015b. Comparative analyses of slope reliability in 3D. Eng. Geol. 196, 12–23.

Lisle, R.J., Leyshon, P.R., 2004. Stereographic Projection Techniques for Geologists and Civil Engineers. Cambridge University Press, New York.

Liu, W.F., Leung, Y.F., 2018. Characterising three-dimensional anisotropic spatial correlation of soil properties through *in situ* test results. Géotechnique 68, 805–819.

Liu, W.F., Leung, Y.F., Lo, M.K., 2017. Integrated framework for characterization of spatial variability of geological profiles. Can. Geotech. J. 54, 47–58.

Lo, M.K., Leung, Y.F., 2017. Probabilistic analyses of slopes and footings with spatially variable soils considering cross-correlation and conditioned random fields. J. Geotech. Geoenviron. 143, 04017044.

Park, H., West, T., 2002. Sampling bias of discontinuity orientation caused by linear sampling technique. Eng. Geol. 66, 99 – 110.

Priest, S.D., 1985. Hemispherical Projection Methods in Rock Mechanics. George Allen and Unwin, London.

Sewell, R.J., Tang, D.L.K., Shaw, R., 2009. Hong Kong geology – A 400 million year journey. Civil Engineering and Development Department, the Hong Kong Government.

Shaw, R., 1997. Variations in sub-tropical deep weathering profiles over the Kowloon Granite, Hong Kong. J. Geol. Soc. 154, 1077–1085.

Shaw, R., Tang, D.L.K., Owen, R.B., Sewell, R.J., 2010. The geological history of Hong Kong. Asian Geographer 27, 43–57.

Storn, R., Price, K., 1997. Differential evolution — a simple and efficient heuristic for global optimization over continuous spaces. J. Global Optim. 11, 341–359.

Strange, P., Shaw, R., 1986. Geology of Hong Kong Island and Kowloon: 1: 20,000 Sheets 11 & 15. 2, Geotechnical Control Office, Civil Engineering Services Department.

Xiao, T., Li, D.Q., Cao, Z.J., Au, S.K., Phoon, K.K., 2016. Three-dimensional slope reliability and risk assessment using auxiliary random finite element method. Comput. Geotech. 79, 146–158.

Xiao, T., Li, D.Q., Cao, Z.J., Zhang, L.M., 2018. CPT-based probabilistic characterization of three-dimensional spatial variability using MLE. J. Geotech. Geoenviron. 144, 04018023.

Zhu, H., Zhang, L.M., 2013. Characterizing geotechnical anisotropic spatial variations using random field theory. Can. Geotech. J. 50, 723–734.

Zhu, H., Zhang, L.M., Xiao, T., 2018. Evaluating the stability of anisotropically deposited soil slopes. Can. Geotech. J. , doi.org/10.1139/cgj–2018–0210 (in press).